Assembly and Characterization of Suspensions for the ERC Speedmeter

Jessie McBrayer Duncan
Supervisor: Dr. Stefan Hild
Institute for Gravitational Research, University of Glasgow
2016 Gravitational IREU Program, University of Florida

August 9, 2016

Abstract

Quantum non-demolition techniques are one way for future gravitational wave detectors to surpass the Standard Quantum Limit. A proof-of-concept experiment at the University of Glasgow seeks to show that a Sagnac speedmeter can significantly outperform a Michelson interferometer with similar design parameters when it comes to quantum noise. Multi-pendulum suspensions will need to be employed in order to isolate the speedmeter's test masses as much as possible from external noise, and these suspensions must be carefully characterized. In this report I will discuss the work I completed in the last two months to assist in the assembly and characterization of these suspensions, as well as the scientific significance of the speedmeter proof-of-concept project as a whole.

1 Introduction

Long ago- long enough for it to take 1.3 billion years for news of the event to reach us- two black holes with a combined mass of around 65 times the mass of our sun spiraled together and collided. This collision stretched and twisted space-time itself, sending ripples out in every direction at the speed of light. This past September, those ripples were detected here on earth by the international LIGO collaboration. For the first time ever, we were able to observe an event by its gravitational wave signature.

Gravitational waves were predicted by Albert Einstein's theory of general relativity, originally published in 1915. When the first detection was announced this year, 100 years later, it announced a new era of astronomy. The field of gravitational physics has never been more exciting. From now on, improvements in detector sensitivity will have very real effects in the number, type, and range of events that we will be able to observe.

1.1 Gravitational Wave Detectors

Gravitational waves are caused by accelerating masses. They propagate out in a wave-like manner, passing freely through matter. As they move they stretch and compress space-time in orthogonal directions. The gravitational wave sources that are plausibly detectable with the current generation of detectors are similar to those detected so far- violent collisions between gigantic compact objects.

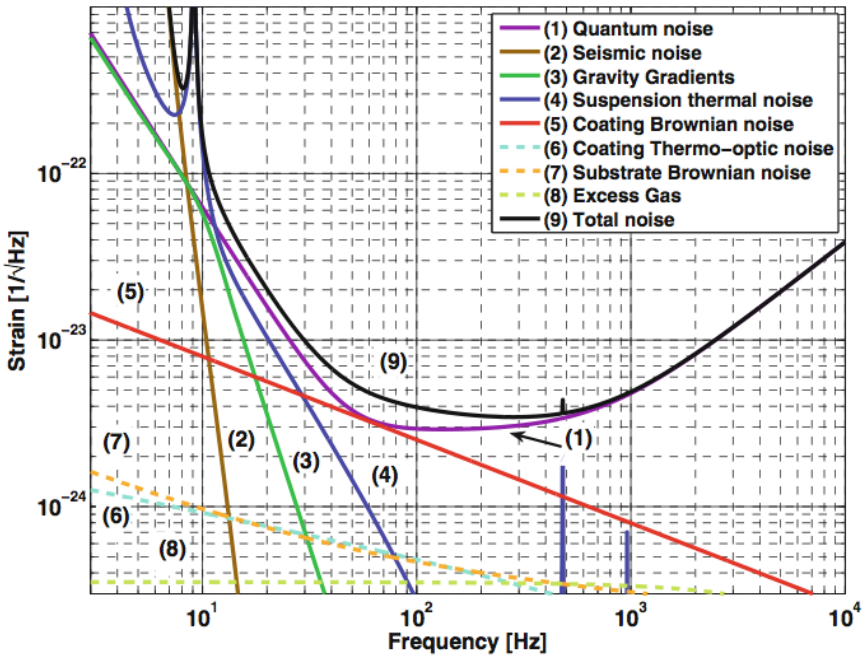

Figure 1: Figure taken from [1], showing amplitude spectral densities of noise components, as denoted by the key. The black line labelled "Total Noise" is the overall instrument sensitivity.

All current gravitational wave detectors are Michelson interferometers- large, L-shaped instruments that utilize the principle of superposition to measure differential length changes between their two arms.

There have been many improvements to the basic Michelson set-up. The addition of Fabry-Perot cavities in the arms of an interferometer can increase the amount of time a photon spends in one of the arms, therefore increasing the instrument's sensitivity to arm length changes. Signal recycling at the dark port of the interferometer allows adjustment to search for signals in varying frequency bands. Power recycling reflects light from the arms back into the instrument again, increasing the total optical power of the instrument without requiring an implausibly high-powered laser [2].

1.2 Thermal, Gravity Gradient, and Seismic Noise

There are varying different limitations posed on the signal to noise ratio (SNR) of an interferometer across the frequency spectrum. Thermal noise is one limiting factor. There are several sources of thermal noise in a typical interferometer set-up, all related to random motion of particles within different materials. You can see several different varieties of thermal noise represented in Figure 1. To minimize thermal noise, it is possible that future detectors might be designed to operate at cryogenic temperatures.

Seismic noise and gravity gradient noise are caused, respectively, by seismic motion of the earth and by density irregularities that cause fluctuations in earth's gravitational field. These noise sources are also displayed in Figure 1. As can be seen, both seismic and gravity gradient noise tend to dominate at low frequencies. Both are remedied by the development of pendulum-style suspension systems. The suspensions used for gravitational wave detectors (and, specifically, the suspensions being built at the University of Glasgow) will be discussed in more detail later in this report.

2 The Speedmeter Concept

2.1 Pursuing the Quantum Limit

As other sources of noise are reduced by current and future advances in instrumentation, modern interferometry will run up against the Standard Quantum Limit (SQL). The SQL is defined by the presence of two different effects- photon shot noise and quantum radiation pressure noise- both of which are directly caused by the quantum nature of light.

Photon shot noise occurs because photons in a laser beam are not equally spaced with respect to time- instead, they follow a Poisson distribution. This causes fluctuations in the signal detected at the end of the beam's path. The fluctuations caused by photon shot noise scale as $\sqrt{P}$, where P signifies the optical power in the interferometer arms. However, as the strength of a gravitational wave signal scales linearly with optical power, the signal to shot noise ratio will actually increase as power is ramped up. The amplitude spectral density for shot noise can be expressed,

$$h_{sn}(f) = \frac{1}{L}\sqrt{\frac{c\hbar\lambda}{2\pi P}} \tag{1}$$

where f is the frequency, λ is the wavelength, c is the speed of light, and L is the interferometer arm length.

Radiation pressure noise is also caused by the irregular distribution of laser photons. Photons have momentum, and therefore transfer momentum onto the mirrors they are reflected by. The inhomogenous distribution of photons causes fluctuations of the force acting on the mirrors within the interferometer, and therefore fluctuations in their positions. The amplitude spectral density for radiation pressure noise is given by,

$$h_{rpn}(f) = \frac{1}{mf^2L}\sqrt{\frac{\hbar P}{2\pi^3 c\lambda}} \tag{2}$$

where m is the mass of the mirror. It can be seen that radiation pressure noise falls off at higher frequencies.

If we define the total quantum noise of our interferometer to be the sum of these two noise sources we can see that shot noise contributes more at high frequencies, while radiation pressure noise dominates at the low. Both radiation pressure noise and shot noise are dependent on optical power as well as frequency, so the shape of the quantum limit can be adjusted by increasing or decreasing the power used. However, any reduction in the quantum noise at higher frequencies that may be gained by using higher power will also cause a decrease in sensitivity at lower frequencies- we can't win over the entire spectrum. This is the equivalent of the Heisenburg Uncertainty Principle, but for interferometry involving uncoupled test masses.

2.2 Speedmeters

Quantum non-demolition techniques are one way to surpass the SQL as experienced by classical interferometers. The speedmeter topology is a non-demolition technique that takes advantage of the fact that, while measurements of positions of uncoupled test masses at different times do not commute, in simple cases their momentums do. As a result of this, if data is recorded that concerns the momentum of test masses in an interferometry setup and not their positions, sensitivity could surpass the SQL over a wide frequency range.

There are several different possible speedmeter configurations. The configuration that has been chosen for a proof of concept experiment at the University of Glasgow is a Sagnac interferometer, shown in comparison with a simple Michelson interferometer in Figure 2.

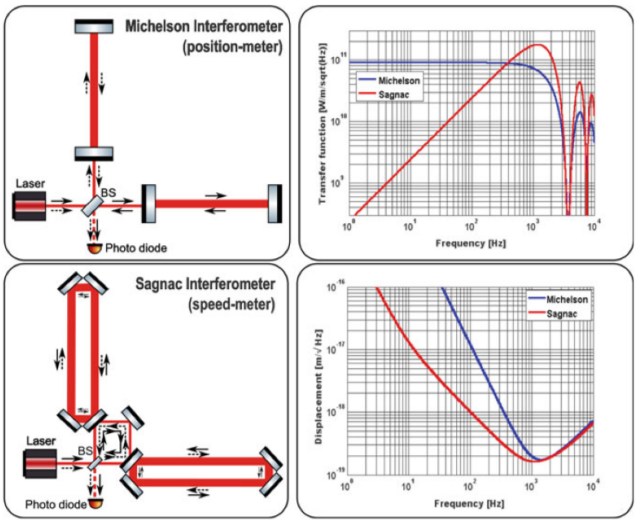

Figure 2: On the left, layout of Michelson and Sagnac interferometers (both with Fabry Perot cavities in the arms). On the right, transfer functions from differential arm length to received signal (*top*) and effective quantum-limited sensitivity (*bottom*) of each instrument [1].

In the traditional Michelson interferometer, individual photons enter only one of the two interferometer arms before being detected- thus, the information gained has to do with the positions of the test masses only. In the Sagnac interferometer, photons travel around both arms. Because of this, each test mass is sensed twice very quickly by two beams moving in opposite directions- a change in position is measured, rather than an absolute position. Due to its ability to extend past the SQL, it is predicted that a Sagnac interferometer could have significantly better sensitivity than a similar instrument utilizing the Michelson configuration [5].

2.3 The 2016 Speedmeter Retreat

The Speedmeter Retreat is a semi-annual meeting of international researchers concerned with the concept of speedmeters in some way, either on the experimental or theoretical side. This summer, I was able to attend the 2016 retreat during the week of June 20th.

The primary subject of discussion this year was that of speedmeter configurations. The Sagnac interferometer I described above is only one purposed

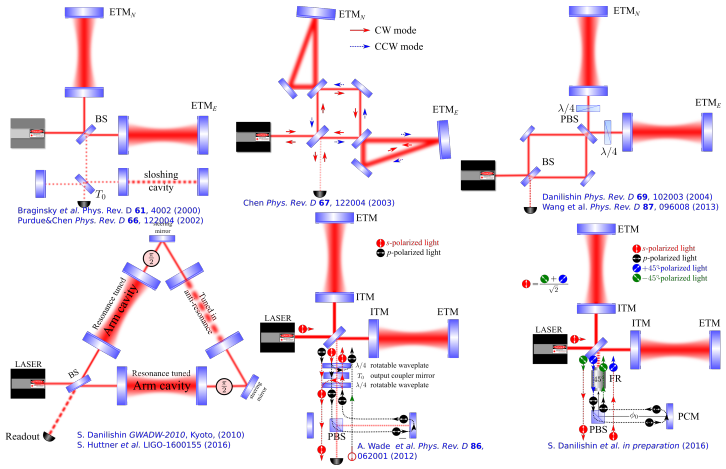

Figure 3: Comparison of currently proposed speedmeter configurations. First (*top left*) we have the classic sloshing speedmeter. The next two (*top middle, top right*) are Sagnac interferometers. On the bottom left, we see an alternative triangular sloshing set up. The last two are examples of how polarization optics could be used to modify an existing Michelson interferometer into *either* a Sagnac or sloshing speedmeter.

method of extracting momentum information from an interferometery set-up without also observing test mass positions. There are 6 main configurations currently proposed, each of which are displayed in Figure 3.

In addition to the classic Sagnac, some of these configurations function essentially as Sagnac interferometers in the sense that light is sent through the interferometer such that it interacts with each test mass twice. The others are based on the concept of signal sloshing.

In a sloshing interferometer, the signal enters an extra 'sloshing cavity' upon exiting the Michelson set-up. The sloshing cavity gives the signal a π phase shift. Therefore, when it is recombined with the signal exiting directly from the Michelson, the total detected signal will consist of the position at time t_2 minus the position at time t_1. A *change* in position is the only measurement extracted, and our interferometer can be considered a speedmeter [3].

Deciding between these configurations for the construction of possible future speedmeters involves both scientific and practical considerations. Some of the designs might be implemented with the addition of relatively few new

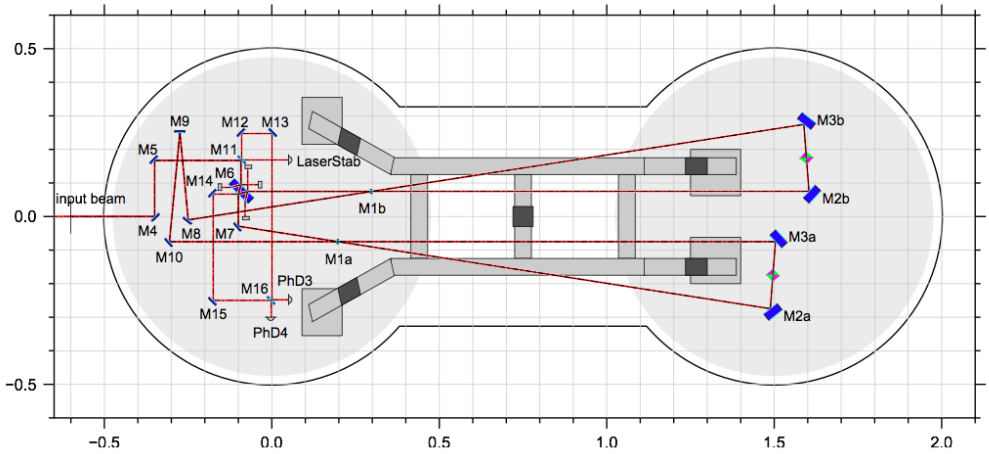

Figure 4: Here we see the optical layout of the speedmeter proof-of-concept. After entering the system from the left, the input beam is split by the main beam splitter (marked 'M6') and guided into the 1.3m arm cavities. The two beams are recombined after circulating the interferometer in opposite directions, and the signal is read out at M16 [7].

components to an existing Michelson interferometer, while others might not have this advantage. The price and reliability of necessary components- especially polarization optics- also deserves consideration. Several papers are in the works coming out of the speedmeter retreat this year, which will explore the feasibility of different designs.

2.4 The ERC Sagnac Speedmeter Project

The European Research Council (ERC) is currently funding a speedmeter proof-of-concept test at the Institute for Gravitational Research within the University of Glasgow. The instrument being built is a Sagnac-type interferometer with triangular arm cavities, housed in two connected vacuum tanks both measuring 1m in diameter. The optical layout of the speedmeter proof-of-concept can be seen in Figure 4. It is expected that the Glasgow speedmeter will outperform an equivalent Michelson at frequencies below 3kHz [6].

My work this summer at the University of Glasgow has been concerned specifically with the suspensions required for the ERC Sagnac Speedmeter.

3 Glasgow Speedmeter Suspensions

Passive isolation can only go so far in preventing noise from an interferometer's surroundings- pendulum-style suspensions are necessary to achieve the level of sensitivity desired in modern interferometry.

When a pendulum is displaced from equilibrium, it experiences a restoring force that tends to return it to its original configuration. The Glasgow suspensions are not simple pendulums- they are multi-stage cascaded pendulum systems. However, they have the same degrees of freedom as any other pendulum- namely:

- motion along the x-axis (longitudinal motion)
- motion along the y axis ('sideways' motion)
- motion along the z-axis (vertical motion)
- rotation around the x-axis (roll)
- rotation around the y-axis (pitch)
- rotation around the z-axis (yaw).

Depending on the structure of a particular suspension, one or more of these degrees of freedom may interact with each other. For example, in a suspension where a mass is suspended from a point vertically displaced from its center of mass, longitudinal and pitch motion will be coupled (i.e. excitation in one will cause excitation in the other).

In this section I will discuss the nature of two of the suspension types employed in the design of the speedmeter proof of concept experiment, which are, respectively, double and triple pendulum suspensions. A full analysis of the dynamics of multi-stage pendulums can be found in [4].

3.1 100g Suspensions

The 100g suspensions were originally designed at Glasgow for the AEI 10m prototype interferometer, and the modifications made to re-use the design for the speedmeter proof-of-concept mainly concern a reduction in the size of the external frames in which the suspensions are mounted. This is necessary due to space limitations posed by the 1m diameter of the speedmeter's vacuum tanks.

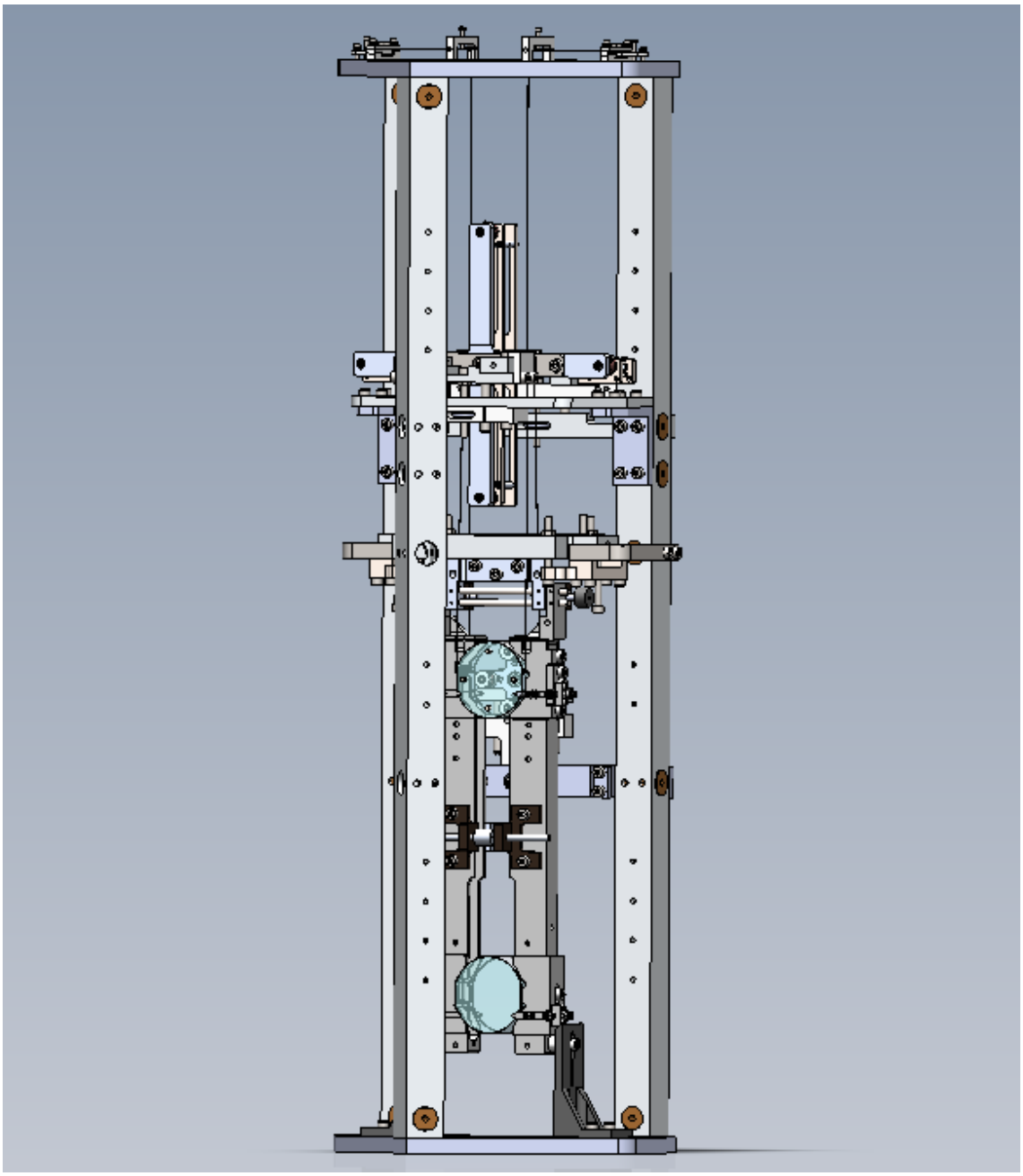

Figure 5: CAD model of the 100g suspensions as they will be built for the speedmeter proof-of-concept. The design is mostly a replica of the 100g suspensions designed at Glasgow for the AEI 10m prototype.

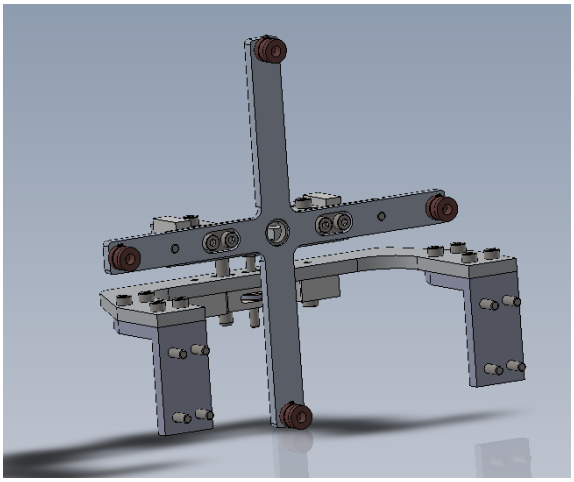

Figure 6: CAD model of the control assembly for the 100g suspensions. This structure is bolted onto the frame from which the suspension hangs. The four copper cups are wound with copper wire and correspond to magnets mounted on the top mass.

These suspensions are triple pendulum suspensions with a fully monolithic bottom stage- that is, the fused silica test mass will be suspended from the second mass by fused silica fibers. This will reduce the thermal noise experienced by the instrument.

The 100g suspensions are controlled using 4 coil-magnet actuators. The placement of the actuators on the control assembly can be seen in Figure 6. Magnets attached to the top mass hang just within copper cups attached to the suspension's frame. Each copper cup is wire-wrapped, allowing the generation of a magnetic field by running a controlled current through the wire. Each of the 4 actuators can be controlled independently.

The actuators actually introduce damping to the top mass even without any intentional current injection. When the top mass moves and the magnets move within the cups, the changing magnetic field induces its own current in the wire, which in turn generates a magnetic field that opposes the motion.

Using these actuators, it is straightforward to inject different kinds of noise into the suspension in order to test its response.

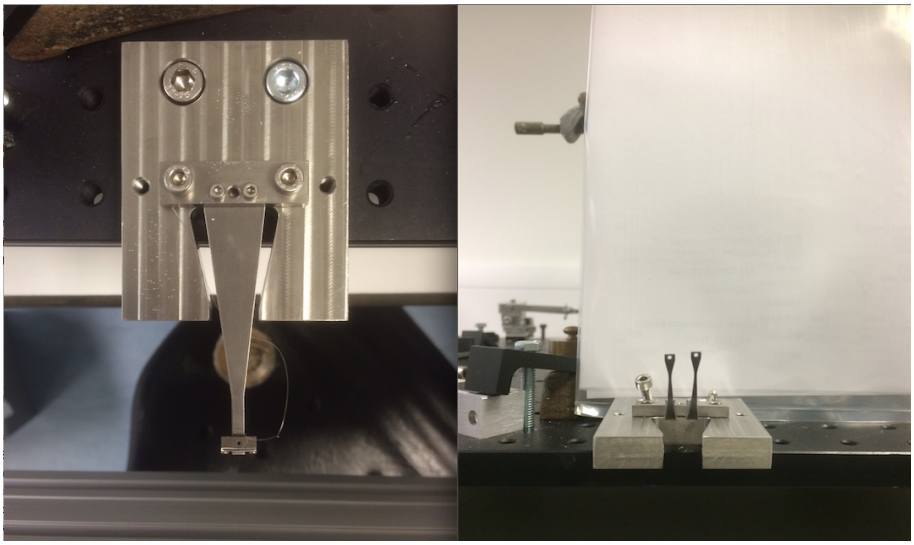

Figure 7: Image of one of the large blade springs under load, showing the housing used to clamp the spring in place (*left*). Two unloaded small blade springs, clamped in the same way, showing their difference in height (*right*).

3.1.1 Blade Springs

Vertical isolation for the 100g suspensions is achieved through the use of two stages of steel blade springs. 28 of these springs have been commissioned for the speedmeter proof-of-concept (14 larger top stage springs and 14 smaller lower stage springs). The experiment design calls for 6 pairs of each type of spring. In order to minimize asymmetry in the vertical isolation, blade pairings need to be decided upon so the two springs in any stage of any of the suspensions will behave as similarly as possible.

In the first weeks of the summer, I made measurements of the unloaded height and displaced height under load of each of the blade springs in order to propose a pairing scheme. The upper springs were loaded with a weight of 200g and the smaller springs with 100g, according to the loads they will respectively experience when the full suspension is assembled as designed.

A digital height measure with a precision of 1/100th of a mm was used to take these measurements, and each spring was measured 6 times in each state. Spring height measurements (both loaded and unloaded) were found to be replicable to within 1/10th of a mm, independent of disassembly and reassembly of their housings (the left of Figure 7 displays the blade housing

Figure 8: Parts for the 100g suspensions shown drying in the clean room.

used for these measurements). The measurements are compiled in a table in Appendix A.

There was significantly more variation between springs than was initially expected, especially with the more flexible lower-stage springs. In Figure 7 the unloaded height difference between two of the smaller blade springs can be seen quite easily. It was also noted that spring stiffness (estimated given the difference in unloaded and loaded heights) and loaded height were not especially correlated.

Therefore, we can choose optimal pairings considering only loaded height, optimal pairings considering only spring stiffness, or any number of intermediary pairings weighted more or less towards one or the other. Procuring a truly optimal blade pairing scheme will therefore require testing of different pairs of springs in the assembled 100g suspension, to see which of these properties has a greater effect on the vertical isolation.

3.1.2 Cleaning and Preparation of 100g Suspension Parts

In light of the blade pairing ambiguity, and to gain experience working with mechanical parts in a clean environment, I spent time over several weeks this summer preparing 100g suspension parts for vacuum. When I arrived, the suspensions were in a dirty assembly, and I was able to assist in disassembling and categorizing the parts for cleaning.

The 100g suspension assemblies contain parts made from aluminum, stainless steel, copper, phosphor bronze, brass, and several types of plastic. Each material has its own requirements for cleaning. Most are cleaned in an ultrasonic bath and then baked in an oven for several days, but the detergents used in the ultrasonic, baking temperature, and time spent in each stage of the process vary. As such the project of cleaning, baking, and wrapping each part for transport is a lengthy logistical process. Figure 8 shows some of the array of different parts I washed, baked, packaged, and labeled for ease of future assembly.

Though the plan at the beginning of the summer was for me to focus mainly on the assembly and testing of the 100g suspensions, the delay in delivery of several parts and general lack of adequate time meant that in the last few weeks of my time in Glasgow I began working with the auxiliary suspensions instead.

3.2 Auxiliary Suspensions

The performance of the auxiliary suspensions used in the speedmeter proof-of-concept will have significantly less effect on the performance of the instrument than that of the cavity optics (the 100g suspensions that support the end test masses, and the 1g input test masses not discussed in this report). Because of this, and to conserve space in the rather cramped vacuum tanks, a double pendulum design suspended from a single post is employed, which can be seen in Figure 9. Though the analysis in [4] deals explicitly with a triple pendulum case, it may be easily modified to consider a double pendulum.

The auxiliary suspensions have 4 coil-magnet actuators in a similar orientation to those of the 100g suspensions, though much more compactly spaced. They, too, can be seen in Figure 9. Longitudinal, pitch, and yaw motion are the inputs most useful for characterizing the behavior of the auxiliary suspensions, and also for beam steering and path length matching. We are able to inject gaussian noise into any of these three inputs, along with other more structured excitations.

3.2.1 Set-up of Spotposition Sensor

To examine the auxiliary suspension's response to various excitations, a spotposition sensor was bolted onto the optical table next to the speedmeter tanks. The optics were set up such that the laser beam was generated outside

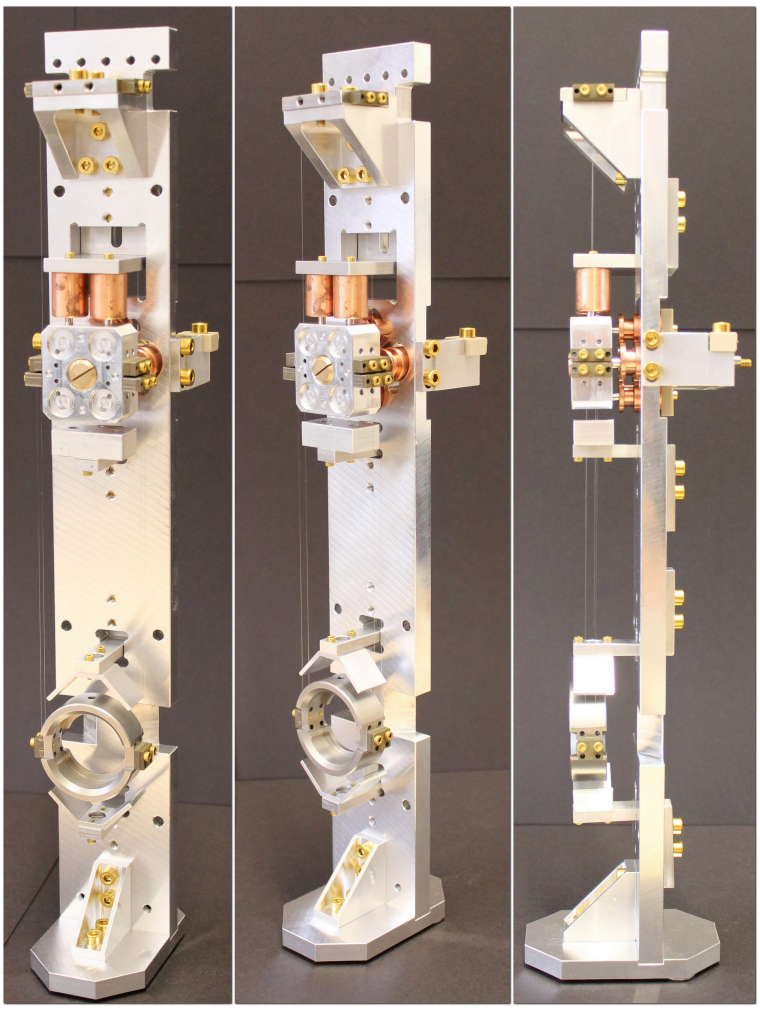

Figure 9: Three angles of the assembled auxiliary suspensions. The coil-magnet actuators can be seen behind the top mass, perhaps best in the angle farthest to the right.

the vacuum, steered into the tank to interact with an auxiliary suspension, and then reflected back out of the tank to be read out by the spotposition sensor.

The spotposition sensor consisted of 4 CCD quadrants. The beam was then aimed as closely as possible to the center of the array. In this way 3 parameters could be recorded at any time: normalized x and y values, as well as the total optical power. Over time, we can see how much the beam shakes in the vertical direction, how strong it is, and how much it shakes in the horizontal direction.

Somewhat intuitively, it can be seen that yaw rotation of the auxiliary suspension's mirror should cause beam motion primarily in the x direction, while pitch should affect the y. After setting up the sensor, this behavior was confirmed by injecting gaussian noise into pitch and yaw and comparing the resulting data with a 'clean' excitation-less dataset.

3.2.2 Longitudinal-Pitch Coupling

When the optics for GEO-600 were first installed and tested, a significant coupling between longitudinal ground motion and pitch motion of the suspended optics was observed [8]. A feedforward system was developed to correct for the excess motion. By exciting the longitudinal mode of the auxiliary suspension and observing its effect on pitch, it might be possible to establish whether that coupling will impact the performance of the speedmeter enough to warrant the development of a similar system at Glasgow.

The mode frequencies expected for long-pitch coupling are given in Appendix A.3. I injected longitudinal sine wave signals at several different frequencies, as well as a swept sine excitation. Figures 10 and 11 display excitation of these modes for an injected sine at 6Hz and a swept sine excitation, respectively.

These results are rather preliminary, and do not yet provide an especially clear picture of how this coupling will eventually effect the performance of these suspensions. Unfortunately my work with the auxiliary suspensions was limited by how late in the summer I began the project. However, given that analysis of data collected concerning this coupling can in fact be done remotely, I am going to present a continuation of this project as a possibility for my senior thesis at my home university this year. In that sense, this report can be considered a report on my progress so far.

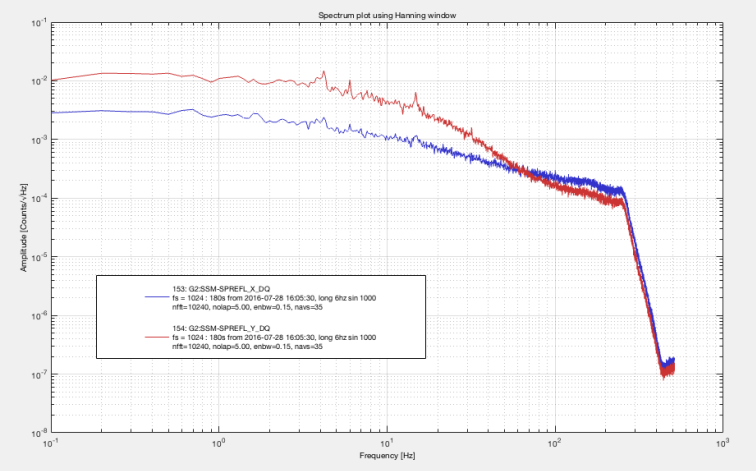

Figure 10: Frequency spectrum for a 6Hz sine longitudinal excitation. Peak in the y (denoted in red) visible at around the 4.35 and 15.8 Hz mode frequencies.

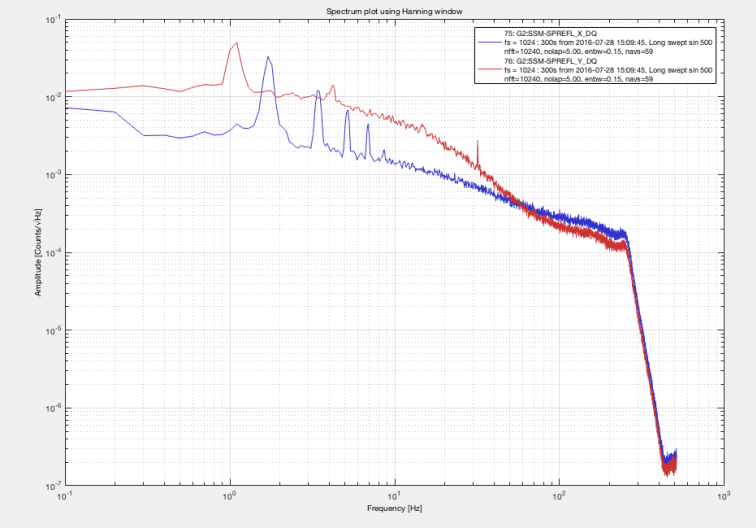

Figure 11: Frequency spectrum for a longitudinal swept sine excitation. Large peak visible in the y at around 1.05, and smaller at around 4.35.

4 Conclusion and Acknowledgements

Although neither of the specific projects I began in Glasgow this summer were able to come to a defined conclusion by the end of my time there, I feel that I have gained a great deal of understanding about optics, interferometry, and the experimental side of the field of gravitational physics in general. I feel, also, that the things I did accomplish will contribute to the overall mission of readying these suspensions for their role in the speedmeter proof-of-concept.

I am extremely grateful to both the NSF and the University of Florida for giving me the opportunity to explore the experimental side of gravitational physics at the University of Glasgow this summer. Thanks especially to Guido Muller, Bernard Whiting, Kristin Nicola, and Ryan Goetz at UF for making this program run so smoothly.

At the IGR, I am especially grateful for all the time spent by my advisor, Dr. Stefan Hild, without whom none of this would have been possible. Thanks also to Jan Henning, Sebastian Steinlechner, Russell Jones, and Teng Zhang for their help and instruction along the way.

Appendices

A Blade Spring Measurements

A.1 Large Blade Springs

Spring Number	Loaded Height(mm)	STDEV	Unloaded Height(mm)	STDEV
1	0.77	0.05	32.72	0.05
2	-0.53	0.04	31.90	0.02
3	0.26	0.04	32.39	0.03
4	1.03	0.05	32.62	0.02
5	0.34	0.02	32.37	0.02
6	1.40	0.01	32.59	0.02
7	0.03	0.05	32.21	0.02
8	1.22	0.02	32.33	0.04
9	0.80	0.06	32.46	0.05
10	1.08	0.05	34.52	0.03
11	1.02	0.05	32.54	0.03
12	1.02	0.04	32.93	0.03
13	0.58	0.03	32.35	0.03
14	-0.07	0.04	32.81	0.03

A.2 Small Blade Springs

Spring Number	Loaded Height (mm)	STDEV	Unloaded Height (mm)	STDEV
1	-0.16	0.02	26.08	0.04
2	1.60	0.02	26.74	0.02
3	1.04	0.03	26.26	0.03
4	1.24	0.03	26.50	0.02
5	-1.15	0.02	26.37	0.02
6	1.17	0.03	26.46	0.03
7	-0.91	0.03	26.37	0.03
8	1.61	0.02	26.68	0.04
9	1.29	0.03	26.16	0.03
10	0.26	0.06	26.51	0.04
11	2.09	0.04	26.46	0.02
12	0.20	0.01	25.97	0.04
13	0.40	0.03	25.53	0.03
14	0.22	0.03	26.27	0.02

A.3 Mode Frequencies (Auxiliary Suspensions)

Mode frequencies expected due to modeling of auxiliary suspension done in [7].

Modes	Frequency in Hz
1.05, 2.68, 4.35, 15.8	pitch + long
1.70, 4.28	yaw

-

References

[1] Stefan Hild. A Basic Introduction to Quantum Noise and Quantum-Non-Demolition Techniques. *Advanced Interferometers and the Search for Gravitational Waves*. Springer International Publishing Switzerland, 2014.

[2] G Hammond, S Hild, M Pitkin. *Advanced technologies for future ground-based, laser-interferometric gravitational wave detectors*. Journal of Modern Optics, 61 (Sup. 1). S10-S45. ISSN 0950-0340.

[3] P Perdue, Y Chen. Practical speed meter designs for QND gravitational-wave interferometers. Physical Review, D66 (2002) 122004.

[4] Callum Torrie. *Development of Suspensions for the GEO 600 Gravitational Wave Detector*. PhD thesis, University of Glasgow, 2001.

[5] Yanbei Chen. Sagnac interferometer as a speed-meter-type, quantum-nondemolition gravitational-wave detector. Physical Review D, 67(12):122004, 2003.

[6] C Grf, B W Barr, A S Bell, F Campbell, A V Cumming, S L Danilishin, N A Gordon, G D Hammond, J Hennig, E A Houston, S H Huttner, R A Jones, S S Leavey, H Lck, J Macarthur, M Marwick, S Rigby, R Schilling, B Sorazu, A Spencer, S Steinlechner, K A Strain, and S Hild. Design of a speed meter interferometer proof-of-principle experiment. Classical and Quantum Gravity, 31(21):215009, 2014.

[7] Jan Henning. *Suspensions for the Glasgow SSM*. Annual Report, University of Glasgow, 2015.

[8] J R Smith, H Grote, M Hewitson, S Hild, H Lu?ck, M Parsons, K A Strain and B Willke. Feedforward correction of mirror misalignment fluctuations for the GEO 600 gravitational wave detector. Classical and Quantum Gravity, (22):3093-3104, 2005.